Enhanced Confinement and Stability in DIII-D Discharges with Reversed Magnetic Shear

E. J. Strait,[1] L. L. Lao,[1] M. E. Mauel,[2] B. W. Rice,[3] T. S. Taylor,[1] K. H. Burrell,[1] M. S. Chu,[1] E. A. Lazarus,[4] T. H. Osborne,[1] S. J. Thompson,[1] and A. D. Turnbull[1]

[1]*General Atomics, P. O. Box 85608, San Diego, California 92186-9784*

[2]*Columbia University, Department of Applied Physics, New York, New York 10027*

[3]*Lawrence Livermore National Laboratory, Livermore, California 94550*

[4]*Oak Ridge National Laboratory, Oak Ridge, Tennessee 37831*

(Received 12 June 1995)

Peaked pressure profiles and central ion temperatures up to 20 keV are observed in DIII-D *H*-mode discharges with a central region of strongly reversed magnetic shear. Short wavelength ballooning modes are stabilized by access to the second stable regime, longer wavelength modes by a conducting wall and possibly by rotational shear. Values of normalized beta, $\beta_N = \beta aB/I$, up to 4 (%-*m*-T/MA), energy confinement are a factor of 3 better than *L* mode, and at least 50% of the noninductive plasma current in this regime demonstrates compatibility with requirements for a steady-state high-beta tokamak power plant.

PACS numbers: 52.55.Fa, 52.25.Fi, 52.35.Py

A major goal of magnetic fusion research is the development of a plasma with both good energy confinement and magnetohydrodynamic (MHD) stability at high beta, leading to a compact, economical fusion reactor. (Here $\beta = 2\mu_0\langle p\rangle/B^2$ is the ratio of plasma pressure to magnetic field pressure.) In addition, this plasma should be consistent with noninductive means of current drive, allowing steady-state operation. The second stable core *VH*-mode configuration [1,2], combining a central region of reversed magnetic shear [3] with the edge transport barrier of very-high-confinement (*VH* mode) plasmas [4], has been proposed as one approach to achieving these goals and is an important element of the DIII-D program [5]. A similar reversed magnetic shear configuration [6] is envisioned as an operating scenario for the Tokamak Physics Experiment (TPX) [7].

The stability of a high beta plasma to both short- and long-wavelength modes is improved by combining reversed magnetic shear with strong toroidal rotation. Reversed magnetic shear allows the plasma to enter the second stable regime for short-wavelength ballooning instabilities. [The magnetic shear $s = (r/q)dq/dr$ is the rate of change of the average pitch of the magnetic field, denoted here by the tokamak safety factor q, with respect to minor radius.] Stabilization of long-wavelength kink modes by a finite conductivity wall with plasma rotations [8] has recently been demonstrated in DIII-D experiments [9,10]. It has also been suggested that reversed shear can improve the energy confinement in the plasma core by stabilizing drift-type microinstabilities [6,11]. Furthermore, the noninductive bootstrap current generated by the pressure gradient in a plasma with low transport rates in the core is consistent with the current density profile needed for magnetic shear reversal, thus reducing the requirements for external current drive [1,2,6].

A central region of reversed shear has been achieved in DIII-D discharges [3] with beta up to 11%, as well as in a number of other tokamaks [12–15]. In many of these earlier experiments the evidence for magnetic shear reversal was indirect since detailed, local measurements of the internal magnetic field were not available. With the recent availability of high-quality measurements of the internal magnetic field, we are now able to report the first observations of high-beta *H*-mode plasmas with improved energy confinement and power plant-relevant ion temperatures in a well-documented core region of magnetic shear reversal. In these experiments the q profile is directly determined from the profile of local field pitch angle measured by a 16-channel motional Stark effect (MSE) diagnostic [16], using information on the plasma shape from external magnetic measurements.

The DIII-D experiments to be discussed here are characterized by an internal transport barrier in the central region of reversed magnetic shear ($dq/dr < 0$). As shown in Fig. 1, there is a strong ion temperature gradient in the region of shear reversal at normalized radius $r/a \leq 0.5$, yielding central temperatures up to 20 keV in cases with low confinement (*L* mode) or high confinement (*H* mode) edges. The ion toroidal rotation velocity is strongly peaked in the same region with a central maximum over 500 km/s, twice the typical value for *VH*-mode discharges with similar input power. The ion temperature and rotation velocity profiles are measured by a 32-channel charge exchange recombination (CER) spectroscopy system [17]. A conventional *VH*-mode discharge with monotonic q profile, also shown in Fig. 1 for comparison, has much broader profiles.

For purposes of transport and stability analysis, the diagnostic data mentioned above are incorporated into detailed equilibrium reconstructions using the EFIT equilibrium code [18]. Input includes MSE data, external magnetic measurements, and pressure profile data including the electron density from Thomson scattering and four CO_2 laser interferometer chords, the electron temperature

0031-9007/95/75(24)/4421(4)$06.00

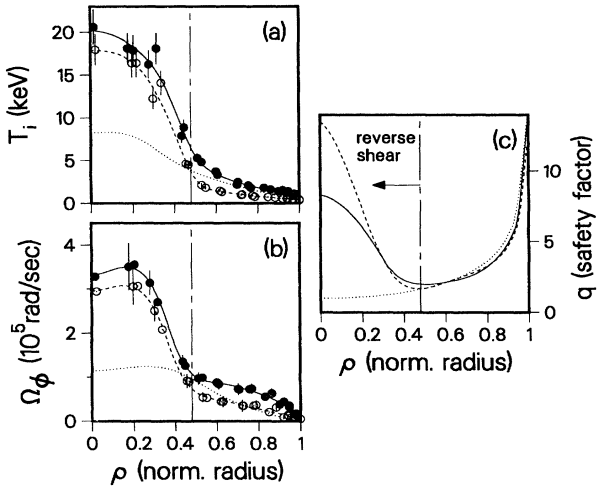

FIG. 1. Measured profiles in L mode with reversed magnetic shear (dashed curves and open circles, discharge 83721 at $t = 1.55$ s); H mode with reversed magnetic shear (solid curves and solid circles, same discharge at $t = 1.66$ s); and VH mode with normal magnetic shear (dotted curves, discharge 78132 at $t = 2.66$ s). Profiles include (a) ion temperature, (b) ion toroidal rotation frequency, and (c) safety factor. A broken vertical line indicates the maximum radius of shear reversal for the first two cases. For all cases: $B = 2.1$ T, $I = 1.6$ MA, and $P_{NB} = 7.7-8.7$ MW.

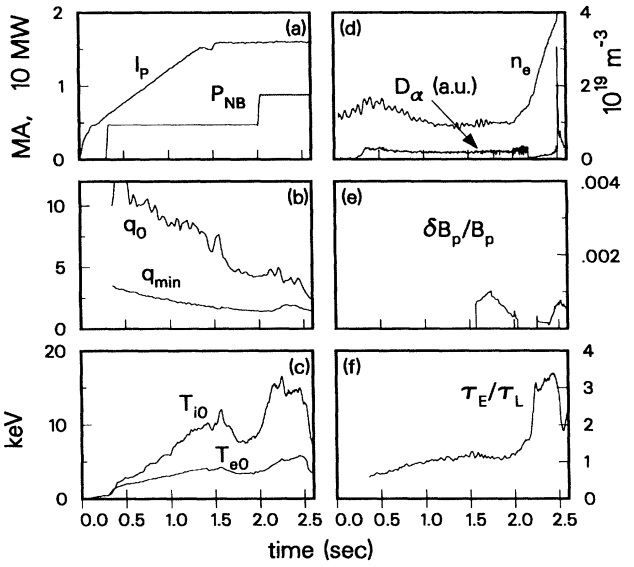

FIG. 2. Time evolution of a reversed central shear discharge: (a) Plasma current and neutral beam power, (b) safety factor at the magnetic axis and minimum value, (c) central ion temperature and electron temperature, (d) line-average density and divertor D_α emission, (e) relative amplitude of MHD activity at the outer wall, and (f) ratio of energy confinement time to L-mode scaling value. Discharge 83729: $B = 2.1$ T, $q_{95} = 5.2$.

from Thomson scattering and electron cyclotron emission, the ion temperature from CER, and Z effective from visible bremsstrahlung radiation. The fast ion pressure profile is calculated assuming classical slowing down of the beam ions; the predicted D-D fusion neutron rate, which includes a large fast-ion contribution, agrees well with measurements.

The reversed central shear configuration was created through programming of the plasma startup in these experiments. The time evolution of such a discharge is shown in Fig. 2, with representative profiles and equilibrium reconstruction in Fig. 3. Here 5 MW of 75 keV deuterium neutral beams are injected early in the plasma current rise of a low-density deuterium discharge [Fig. 2(a)] in order to raise the electron temperature [Figs. 2(c) and 3(a)] and slow the inward penetration of the inductively driven current. This leads to off-axis accumulation of current density and shear reversal near the axis [Fig. 3(c)], with the central safety factor q_0 remaining above the minimum value $q_{\min}$ [Fig. 2(b)]. A flattening of the poloidal field profile near the magnetic axis [Fig. 3(e)] is characteristic of the reversed magnetic shear. The experimentally inferred noninductive current [19] contributes at least 50% of the total plasma current, and transport analysis confirms that both neutral beam-driven current and the bootstrap current associated with the large internal pressure gradient are peaked away from the magnetic axis, as needed to sustain the shear reversal. Further control over the current density profile can be gained by modifying the edge plasma through the timing of the L-to-H mode transition [shown in Fig. 2(d) by the drop in D_α emission at $t = 2.17$ s]. These transient techniques permit the reversed central shear configuration to be studied with existing resources, and may also prove useful in the initial formation of a reversed central shear plasma to be sustained in steady state by noninductive current drive.

There is a clear reduction in the measured transport in many of the reversed magnetic shear discharges. Reduced transport can be inferred directly from the increased ion temperature gradient shown in Figs. 1 and 3, in comparison to similar discharges without reversed magnetic shear. The region of reversed shear and improved confinement typically occupies the central 20–30% of the plasma volume, and is observed in discharges with (H mode) or without (L mode) an edge transport barrier. The energy confinement time reaches values approximately 3 times the prediction of an empirical scaling law [20] for L-mode discharges; this is comparable to VH-mode values [4] [see Fig. 2(f)], but without the large rotational shear in the vicinity of $0.6 \leq r/a \leq 0.8$, which is characteristic of VH-mode discharges. Instead, the large gradients of ion temperature and rotation lie at smaller radius, in the region of magnetic shear reversal. Detailed transport analysis using the ONETWO code [21] for the case in Fig. 3 shows that the ion thermal diffusivity in the reversed shear region is reduced to near the neoclassical value. However, comparison to the neoclassical prediction is complicated by uncertainties in neutral beam power deposition and charge exchange losses arising from low plasma density, and by the questionable validity of standard neoclassical transport

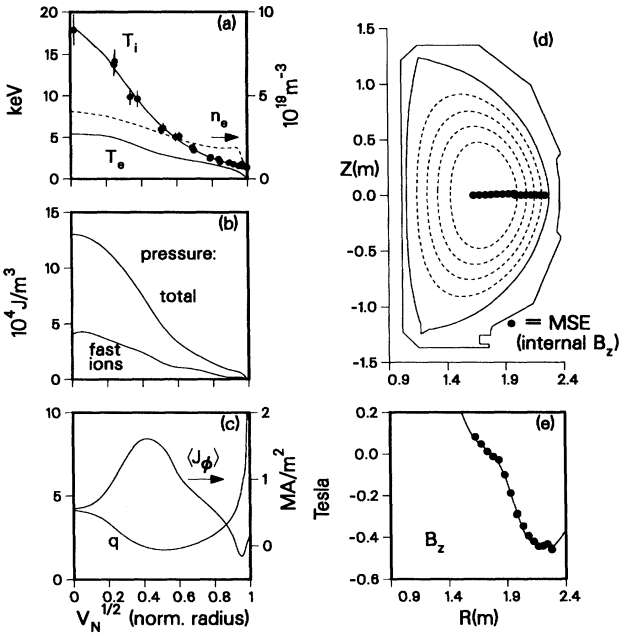

FIG. 3. Measured profiles and equilibrium reconstruction for same discharge as Fig. 2: (a) Ion temperature, electron temperature, and electron density; (b) total pressure and fast ion pressure; (c) safety factor and flux-surface averaged current density; (d) poloidal flux surfaces with MSE measurement locations; and (e) measured and fitted profiles of internal poloidal field. Radial coordinates are (a)–(c) square root of normalized volume within a magnetic flux surface and (d), (e) major radius. Discharge 83729 at $t = 2.25$ s.

theory in the steep gradient region where the temperature gradient scale length approaches the ion poloidal gyroradius.

Most of the plasma volume is calculated to be in the second stable regime for ideal MHD ballooning modes, as expected, because of negative magnetic shear at small radius and positive but weak magnetic shear at intermediate radius. Analysis with the CAMINO stability code [22], as shown in Fig. 4(a), indicates that the discharge has access to the second stable regime everywhere except for a narrow region with a normalized radius near 0.9. At the later analysis time, near maximum beta, the measured pressure gradient has reached the stability limit in that region but remains free to increase everywhere else. In contrast, with a monotonic q profile ballooning modes would be unstable from the center out to the radius of peak pressure gradient [Fig. 4(b)].

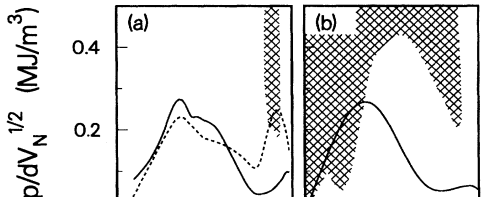

FIG. 4. Ideal ballooning stability limits for same discharge as Figs. 2 and 3: (a) Measured pressure gradient profiles early in H mode (solid curve, $t = 2.25$ s, $\beta = 2.1\% = 1.7\ I/aB$) and late in H mode (dashed curve, $t = 2.45$ s, $\beta = 3.3\% = 2.7\ I/aB$), with the calculated region of instability (shaded); and (b) pressure gradient and stability limit assuming a monotonic q profile (same discharge, $t = 2.25$ s).

Strong rotational shear may be important for stabilization of reversed magnetic shear discharges against resistive instabilities [23]. In particular, a significant difference in rotation rates between pairs of flux surfaces with the same q value, as in the profiles of Fig. 1, is calculated to stabilize double tearing modes. During an interval free of MHD activity [see Fig. 2(e), $t = 2.15$ s] resistive stability calculations using the MARS code [8,24] indicate that the plasma is unstable if it does not rotate, but is stable with the measured plasma rotation. As shown in Fig. 2(e), periods of MHD instability still occur that may be correlated with $q_{\min}$ reaching integer values, particularly $q_{\min} \approx 2$. These instabilities have rapid growth rates and are thought to be infernal modes [25]; control of $q_{\min}$ away from integer values is calculated to give stability against these modes.

Long-wavelength ideal instabilities ultimately limit the high confinement phase of the discharge shown in Figs. 2–4. Calculations using the GATO code [26] with a conducting wall at the position of the DIII-D vacuum vessel predict that at maximum beta ($t = 2.45$ s) the plasma is stable to ideal kink modes with toroidal mode numbers $n = 1$ and $n = 3$, but only marginally stable to the $n = 2$ kink mode. The calculated instability is localized near the edge of the plasma, and is likely unrelated to the reversed magnetic shear in the core. A rapid MHD instability correlated with the D_α spike at $t = 2.5$ s [see Fig. 2(d)] halts the rise of beta, and corresponds well in growth rate, mode number, and radial location to the calculated instability. A similar low-n kink-ballooning mode destabilized by the large current density and pressure gradient near the edge ($r/a > 0.9$) has previously been identified as responsible for the termination of VH mode [27].

The beta limit imposed by low-n instabilities is sensitive to the details of the current density distribution in the outer part of the plasma, and high values of beta should be possible by controlling the current profile. In most discharges of the series described here, the maximum beta value normalized to the Troyon beta limit scaling was $\beta_N = \beta/(I/aB) \approx 2.7$ (%-m-T/MA), a value typical of many VH-mode discharges but significantly smaller than the values of 3.5 to 6 achieved in some DIII-D discharges. However, higher values of β_N with reversed central shear were reached in discharges where programming of the early discharge evolution yielded a lower current density and pressure gradient at the plasma edge, while maintaining low internal inductance which is favorable for wall stabilization. As shown in Fig. 5(b),

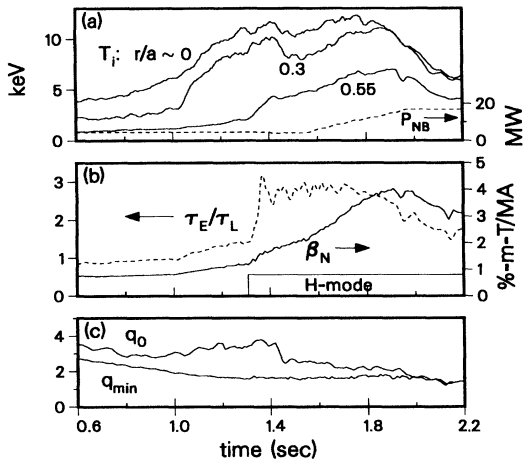

FIG. 5. High-beta reversed central shear discharge: (a) Ion temperature at major radius $R = 1.77$, 1.89, and 2.04 m, corresponding to $r/a \approx 0$, 0.3, and 0.55, and neutral beam power; (b) normalized beta, $\beta_N = \beta(I/aB)^{-1}$, and ratio of energy confinement time to L-mode scaling value; and (c) safety factor at the magnetic axis and minimum value. Discharge 84736: $B = 1.6$ T, $q_{95} = 5.9$, $\beta \leq 5.1\%$.

values of β_N up to 4.0 were reached, corresponding to central beta values up to 15%.

Although reversed magnetic shear appears to be a necessary condition for the enhanced central confinement observed in these discharges, reversed shear alone is not sufficient, as shown in Fig. 5. Here the shear reversal ($q_0 > q_{\min}$) occurs early in the discharge but the internal transport barrier forms later, as shown by a sudden rise in central ion temperature and temperature gradient beginning at $t = 1.05$ s. At the same time, energy confinement [Fig. 5(b)] rises to 1.4 times the L-mode value, before the L to H transition at $t = 1.3$ s. (A smaller plasma current and toroidal field here lead to lower ion temperatures than in Figs. 1–3.) The transport barrier is then maintained as $q(0)$ decreases, until the terminating instability at $t = 1.9$ s. We speculate that the transport barrier may require a minimum radius of the reversed shear region, perhaps on the order of the ion poloidal gyroradius. Stabilization of turbulence by the sheared $\mathbf{E} \times \mathbf{B}$ flow associated with the strong rotational velocity shear may also play a role in creating or maintaining the thermal transport barrier [28].

The discharges described here demonstrate the potential benefits of reversed central shear for high-beta, high-confinement, steady-state tokamak configurations. The internal transport barrier leads to good central confinement, high central ion temperatures, and central peaking of the ion pressure, which is favorable for a high fusion rate. The addition of an H-mode edge transport barrier improves global confinement, but reversed magnetic shear with a relatively cool L-mode edge may also be an attractive option. Reversed magnetic shear stabilizes short-wavelength ballooning modes, while the nearby vacuum vessel stabilizes long-wavelength kink modes, given plasma rotation and a sufficiently broad current density profile. Strong shear of the rotational velocity and avoidance of integer values of $q_{\min}$ are also calculated to improve the stability. Planned experiments will explore the transport and stability properties of this configuration, and will sustain it for long pulses with off-axis noninductive current driven by high power microwaves.

This is a report of work supported by the U.S. Department of Energy under Contracts No. DE-AC03-89ER51114, No. W-7405-ENG-48, No. DE-AC05-84OR21400, and No. DE-FG02-89ER53297.

[1] T. S. Taylor *et al.*, Bull. Am. Phys. Soc. **38**, 1936 (1993).
[2] A. D. Turnbull *et al.*, Phys. Rev. Lett. **74**, 718 (1995).
[3] E. A. Lazarus *et al.*, Phys. Fluids B **3**, 2220 (1991); **4**, 3644 (1992).
[4] G. L. Jackson *et al.*, Phys. Rev. Lett. **67**, 3098 (1991).
[5] T. S. Taylor *et al.*, Plasma Phys. Controlled Fusion **36**, B229 (1994).
[6] C. Kessel *et al.*, Phys. Rev. Lett. **72**, 1212 (1994).
[7] R. J. Goldston *et al.*, in *Proceedings of the 20th EPS Conference on Controlled Fusion and Plasma Physics, Lisbon, 1993* (European Physical Society, Petit-Lancy, 1993), Vol. 17C, Part I, p. 319.
[8] A. Bondeson and D. J. Ward, Phys. Rev. Lett. **72**, 2709 (1994).
[9] E. J. Strait *et al.*, Phys. Rev. Lett. **74**, 2483 (1995).
[10] T. S. Taylor *et al.*, Phys. Plasmas **2**, 2390 (1995).
[11] B. B. Kadomtsev and O. P. Pogutse, Sov. Phys. JETP **24**, 1172 (1967).
[12] M. Hugon *et al.*, Nucl. Fusion **32**, 33 (1992).
[13] G. T. Hoang *et al.*, Nucl. Fusion **34**, 75 (1994).
[14] Y. Kamada *et al.*, Nucl. Fusion **34**, 1605 (1994).
[15] R. J. Goldston *et al.*, Plasma Phys. Controlled Fusion **36**, B213 (1994).
[16] B. W. Rice, D. G. Nilson, and D. Wroblewski, Rev. Sci. Instrum. **66**, 373 (1995).
[17] P. Gohil *et al.*, in *Proceedings of the 14th IEEE/NPSS Symposium on Fusion Technology* (Institute of Electrical and Electronics Engineers, Piscataway, NJ, 1992), Vol. II, p. 1199.
[18] L. L. Lao *et al.*, Nucl. Fusion **30**, 1035 (1990).
[19] C. B. Forest *et al.*, Phys. Rev. Lett. **73**, 2444 (1994).
[20] P. N. Yushmanov *et al.*, Nucl. Fusion **30**, 1999 (1990).
[21] H. St. John *et al.*, in *Proceedings of the 20th EPS Conference on Lisbon, 1993* (European Physical Society, Petit-Lancy, 1993), Vol. 18B, Part I, p. 99.
[22] M. S. Chance *et al.*, in *Proceedings of the Workshop on Theory of Fusion Plasmas, Varenna, Italy* (Editrice Cmpositori, Bologna, 1987), p. 87.
[23] R. L. Dewar and M. Persson, Phys. Fluids B **5**, 4273 (1993).
[24] M. S. Chu *et al.*, Phys. Plasmas **2**, 2236 (1995).
[25] J. Manickam *et al.*, Nucl. Fusion **27**, 1461 (1987).
[26] L. C. Bernard *et al.*, Comput. Phys. Commun. **24**, 377 (1981).
[27] E. J. Strait *et al.*, in *Proceedings of the 20th EPS Conference on Controlled Fusion and Plasma Physics, Lisbon, 1993* (Ref. [7]), Vol. 18B, Part I, p. 211.
[28] K. H. Burrell, Plasma Phys. Controlled Fusion **36**, 291 (1994).